Asian Journal of Chemistry; Vol. 28, No. 10 (2016), 2246-2254

ASIAN JOURNAL OF CHEMISTRY

http://dx.doi.org/10.14233/ajchem.2016.19961

Adsorption of Aqueous Mercury by Amide-Functionalized Ordered Mesoporous Carbon

JIANZHONG ZHU[1,*], DONGLIANG JI[1], BAOLIN DENG[2], JOHN YANG[3], YING DING[1] and YA SU[1]

[1]Key Laboratory of Integrated Regulation and Resource Development on Shallow Lake of Ministry of Education, College of Environment, Hohai University, Nanjing 210098, P.R. China
[2]Department of Civil and Environmental Engineering, University of Missouri, Columbia, MO 65211, USA
[3]Center of Environmental Sciences, Lincoln University of Missouri, Jefferson City, MO 65102, USA

*Corresponding author: E-mail: zhuhhai2010@hhu.edu.cn

Received: 10 March 2016; *Accepted*: 23 May 2016; *Published online*: 30 June 2016; AJC-17976

Amide-functionalized ordered mesoporous carbon was developed for removal of mercury (Hg^{2+}) from aqueous phase. Ordered mesoporous carbon was synthesized using a mesoporous silica template, SBA-15, followed by *in situ* polymerization of acrylic acid, carbonization and template removal. Ordered mesoporous carbon was subsequently functionalized with ethylenediamine through a combined treatment of nitric acid and thionyl chloride. Physio-chemical properties of the carbons were characterized by scanning electron microscopy, transmission electron microscopy, X-ray diffraction, Fourier transform IR spectroscopy, potentiometry and N_2-adsorption/desorption (BET). Adsorption kinetics and equilibrium of Hg was assessed in batch experimental systems. Results indicated that amide-functionalized carbon (FOMC) maintained the original ordered mesoporous structure and hexagonal framework with an averaged surface area of 607 m^2 g^{-1}, pore size of 4.1 nm and pore volume of 0.62 cm^3 g^{-1}. The functionalization process immobilized significant amounts of amide group on the carbon surface and enhanced surface negative charges and hydrophilicity. The adsorption of mercury(II) by functionalized ordered mesoporous carbon reached equilibrium within 480 min. The adsorption capacity was 1.5-time as large as for ordered mesoporous carbon, suggesting an enhanced affinity of surface amide groups for aqueous Hg binding. The adsorption also occurred in a wider pH range (about 5.0-7.0 *vs*. 5.5-6.5). The Freundlich adsorption model fitted the isotherms reasonably well. A surface complexation double layer model was developed to describe the Hg^{2+} adsorption, from which related H^+ and Hg^{2+} binding constants on the surface were obtained.

Keywords: Ordered mesoporous carbon, Surface modification, Mercury adsorption, Surface complexation model.

INTRODUCTION

The recent success of synthesizing ordered mesoporous materials [1-5] has drawn much attention to their potential industrial and environmental applications. Ordered mesoporous materials (OMCs) have regular arrays of uniform nanopores and high specific surface areas that could be explored for efficient adsorption of toxic metals from the aqueous phase [6]. Their applications as an absorbent usually require functionalization with organic or inorganic compounds, which modifies the surface hydrophobicity or hydrophilicity and allows adsorption to be specific to target contaminants [7-9].

Functionalization of carbon materials can be achieved through surface oxidization using oxidative agents such as nitric acid, ozone, or ammonium persulfate, followed by the substitution of oxidative groups by functionalities containing heteroatoms such as N and S groups [10-13]. For practical applications, such surface modification needs to be specific to target contaminants. The adsorptive characteristics of functionalized carbons for target contaminants depend on specific interactions between contaminants and surface functional groups [14,15]. For example, modifications that enhance surface hydrophilicity could generate new surface sites and increase the metal adsorption from the aqueous phase through electrostatic interactions and/or covalent bindings. Functionalized mesoporous carbons were reported to show high adsorptive capacities for chromate and arsentate anions [16] and other metal ions such as Fe^{3+} and Cu^{2+} [17-23]. The modification of activated carbon by amide groups was found to enhance Hg^{2+} ion adsorption from the aqueous phase [24].

Mercury is a toxic metal in the environment. Human exposure to mercury at high levels can cause damages to brain, heart, kidneys, lungs and immune system. The goal of this study is to explore the use an OMC-based absorbent for enhanced aqueous mercury ion (Hg^{2+}) removal. Specific objectives are to: (i) functionalized OMC with amide-functional groups, a high-affinity ligand for Hg binding; (ii) characterize the physiochemical surface properties of the functionalized carbon; (iii) determine the adsorptive kinetics and capacities for Hg^{2+} removal; and (iv) model the experimental data by the

diffuse double layer model (DLM) using a computer program, FITEQL 4.0. The model development is important to predict the behaviours of reactive contaminants in the environment and understand the adsorption mechanisms. Surface complexation models (SCM) including double layer model have been used to describe aqueous Hg^{2+} adsorption that changes as a function of pH [25,26] and applied successfully to the binding site analysis of kaolinite, natural organic materials, bacterial surface [27-33] and carbon adsorbents [34-36]. In the surface complexation models modeling, the surface complexation constants that best fits the Hg adsorption data on the functionalized carbon could be generated using a non-linear least-square regression approach [37,38].

EXPERIMENTAL

Synthesis and functionalization of ordered mesoporous carbon: An ordered mesoporous carbon (OMC) was synthesized by a procedure previously described [39], based on the use of mesoporous silica (SBA-15) as a template. As illustrated in Fig. 1, the synthesized OMC was subsequently oxidized with nitric acid, chlorinated using thionyl chloride, then functionalized with ethylene diamine [39]. Specifically, OMC, 2.5 g, was slowly added to 25 mL of 4 M nitric acid, heated and stirred for 120 min at 50 °C, then filtered and air-dried. The oxidized OMC was refluxed with 5 % $SOCl_2$ in toluene solution at 70 °C for 6 h, then filtered and air-dried. Subsequently, the chlorinated OMC was refluxed in 40 mL toluene containing 0.05M ethylene diamine for 4 h, filtered and extracted for 2 h with toluene, then oven-dried overnight at 40 °C under vacuum [40].

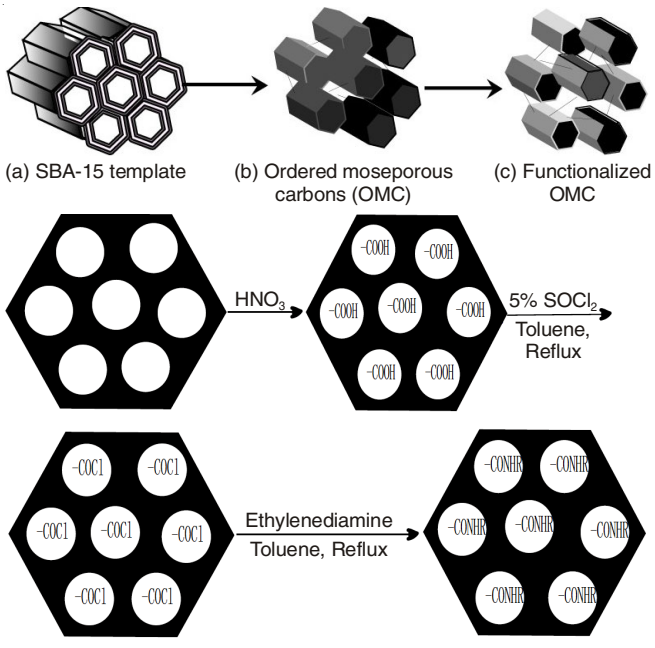

Fig. 1. An illustration of synthesis and functionalization of ordered mesoporous carbon

Physico-chemical characterizations: The amide-functionalized OMC (FMOC) was characterized by an AMRAY 1600 scanning electron microscope (SEM) and a JEOL 2010 high-resolution transmission electron microscope (TEM) to evaluate the alterations of surface morphology by the treatments. The porous properties were determined by nitrogen (N_2) adsorption-desorption using a PMI Automated BET sorptometer. The crystal structures were analyzed by a MiniFlex automated, microprocessor-controlled X-ray powder diffractometer (XRD). A Nicolet 4700 Fourier transform IR spectrometer was used to qualitatively measure the surface contents of organic-inorganic ligands. The elemental compositions were analyzed by a Perkin Elmer 2400 Series II CHNS/O elemental analyzer.

Surface charges and proton-binding isotherms were evaluated by potentiometry. The carbon samples, 0.100 ± 0.001 g, was suspended in 50 mL of 0.1 N $NaNO_3$ and acidified with 2 mL of 0.1 N HNO_3. The suspension was purged under a constant N_2 gas flow to eliminate the influence of atmospheric CO_2 and stirred magnetically throughout the measurements. Titration was carried out using 0.1 M NaOH by a Titrino computer-controlled 798 microburette with Datalog software. The solution pH was measured by a Ross pH electrode after 10 min of equilibration. Mean surface charge as a function of pH (2.0 to 11.0) was calculated from the difference between the total base or acid added and the equilibrium OH^- or H^+ ion concentration for a given quantity of carbon as shown in eqns. 1 and 2:

$$Q_{(OMC)} = \frac{[-COH_2^+]-[-CO^-]}{a_{OMC}} = \frac{(C_A - C_B + [OH^-]_e - [H^+]_e)(V_0 + V_t)}{m_{OMC}} \quad (1)$$

$$Q_{(FOMC)} = \frac{[\equiv CFOH_2^+]+[-COH_2^+]-[\equiv CFO^-]-[-CO^-]}{a_{FOMC}} = \frac{(C_A - C_B + [OH^-]_e - [H^+]_e)(V_0 - V_t)}{m_{FOMC}} \quad (2)$$

where [ ] indicates concentrations of solute and surface species per unit volume of solution (V), C_A and C_B are added acid and base concentrations, respectively and V_0 and V_t are the volumes of background electrolyte and titrant added, respectively. m is the mass of adsorbent. $[H^+]_e$ and $[OH^-]_e$ are the proton and hydroxyl concentrations at equilibrium, calculated from the measured pH. Activity coefficients in the solution were estimated using the Davis' Equation.

Adsorption experiments: Batch experiments were conducted in duplicates to determine the adsorption kinetics and equilibrium isotherm for Hg^{2+} removal by the carbons. In the kinetics study, a carbon sample, 0.1000 g, was added to a 500-mL glass flask containing 300 mL of a phosphate buffer solution (pH ~ 6.0) with initial concentrations of 30 and 50 mg Hg L^{-1}, respectively. The suspensions were shaken at 150 rpm and 25 °C. Samples, 10 mL each, were taken using a plastic syringe at intervals of 2, 5, 10, 30, 60 min and then every 60 min up to 1440 min. Each sample was filtered through a Whatman 0.45 um syringe filter and the filtrate was acidified with 2-3 drops of concentrated HNO_3 before Hg^{2+} analysis by a VARIAN ICP-OES spectrometer. The equilibrium isotherms were established by adding predetermined amounts of carbon to 60 mL glass bottles with Hg concentrations varying from 50 to 120 mg L^{-1}. The effect of pH, ionic strength and inter-

fering ions on the Hg^{2+} adsorption were also investigated. The suspensions were shaken at 150 rpm and 25 °C for 24 h before sampled and analyzed for Hg by ICP. The solution pH was measured using an Orion 525A pH meter. The quantity of mercury adsorbed per unit carbon mass was calculated by dividing the difference between initial and residual amounts of mercury in the solution by the carbon loading.

A mercury standard stock solution was prepared by dissolving a known quantity of $Hg(NO_3)_2$ in distilled water and acidifying with concentrated HNO_3 to prevent hydrolysis. For QA/QC, the ICP-OES was automatically calibrated using mercury standards (SPEX Certiprep, NJ) for every 10-sample run and spike standards were also checked during the analyses. The Hg standard recovery was in the range of 91.3-108.7 % and the variation among replicated samples was within ± 10 %.

Surface complexation modeling: Surface complexation models (SCMs) have been extensively used for describing metal adsorption or surface acid-base reactions [41-44], especially the adsorption of ionic species on charged surfaces [45-48]. The diffuse layer model (DLM) of surface complexation models was reported to be used for the sorption of organic ligands and metals onto porous adsorbents [49]. In double layer model, it is assumed that the surface charges consist of permanent charges (written as $\equiv X^-$), ligand-associated charges (written as ≡XL) and pH-dependent charge of amphoteric hydroxyl groups (written as ≡SOH) [49-52]. Furthermore, the oxidized functional groups on the surface were assumed to be not occupied by the organic ligands. Therefore, in this case, the surface site concentrations of ≡XL, $\equiv X^-$ and ≡SOH could be estimated using the potentiometric titration curve and the ligand loading data. For FOMCs, the equilibrium constants (log K) of the XL groups in solution were calculated and used in the fitting process [37].

The Hg adsorption data were modeled in this study by assuming the Hg binding at the $\equiv SO^-$, $\equiv X^-$ and ≡XL charge sites on the surface. The surface precipitation of mercury was neglected [53]. The modeling was adapted from previous successful applications for the adsorption of metals and organics on various adsorbents [54-57]. The Hg adsorption as a function of solution pH, aqueous Hg concentration and surface acidity were used as inputs and the model parameters were calculated based on a diffuse layer model using FITEQL software for the best fit of the experimental data [37].

RESULTS AND DISCUSSION

Physico-chemical characterizations: SEM micrographs indicated that OMC surfaces (Fig. 2A-a) consisted of isolated, ball-like particles while FOMC (Fig. 2A-b) exhibited irregularly-shaped, particle-like morphology with disordered particle clusters. After the Hg adsorption, FOMC-Hg (Fig. 2A-c) had a few dark areas with various dimensions and shapes that were likely associated with adsorbed Hg^{2+} ions [24]. In TEM micrographs, the SBA-15 template (Fig. 2B-a) clearly showed long-range orders of uniform mesoporous structures, demonstrating well-ordered (100) and (110) hexagonal arrays of silica nanorods [39]. Ordered mesoporous carbon (Fig. 2B-b) maintained the highly-ordered 2-D hexagonal symmetry of the SBA-15 template. Distances between the centers of adjacent nanorods were measured to be 10.0 nm in SBA-15 and ~8.0 nm in OMC. The functionalization of OMC resulted in some loss of the

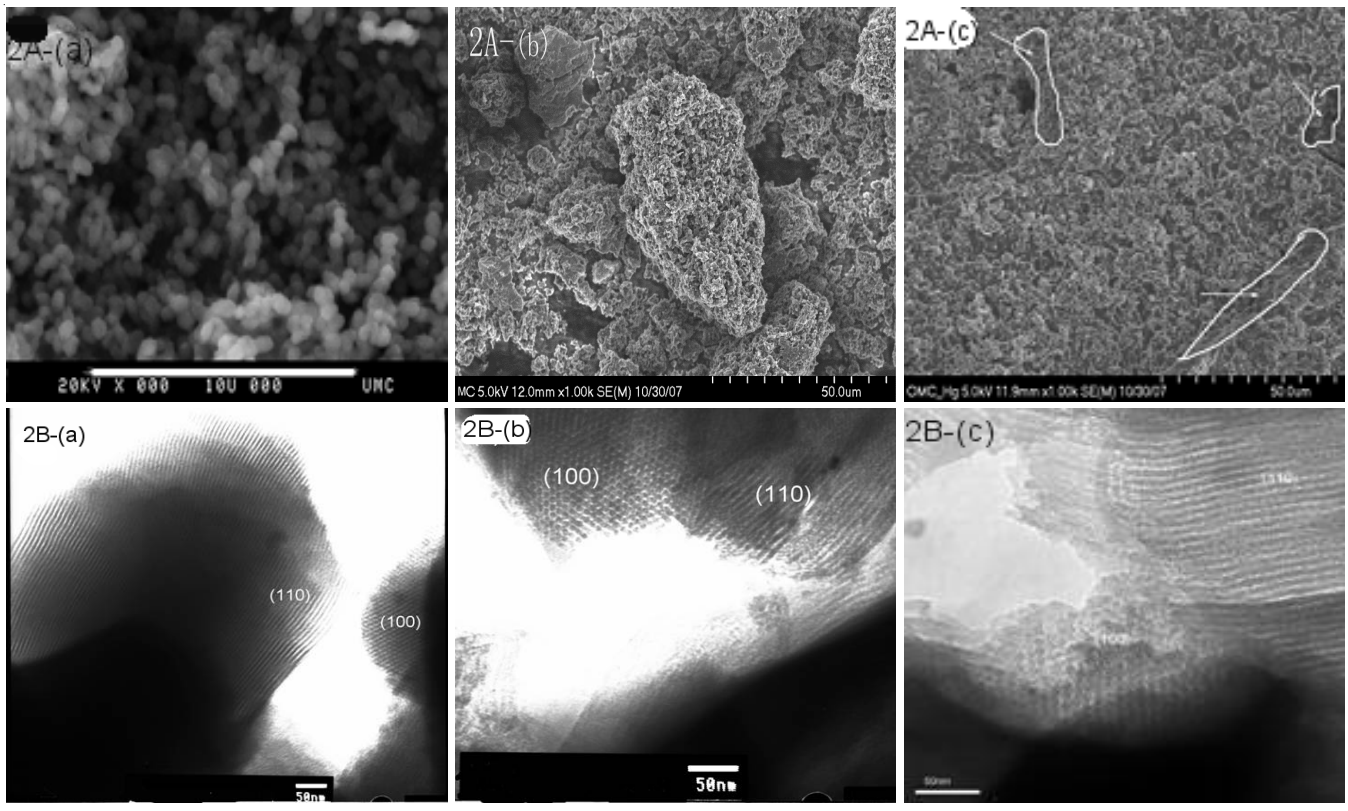

Fig. 2. SEM (A) micrographs of OMC (2A-a), FOMC (2A-b), FOMC-Hg (2A-c) and TEM (B) micrographs of SBA-15 (2B-a), OMC (2B-b) and FOMC (2B-c)

2-D hexagonal symmetry in FOMC (Fig. 2B-c), which may reflect the impacts of chemical treatments on the structure, but the order and uniformity of mesoporous structures was still maintained.

XRD patterns (Fig. 3) indicated that SBA-15 exhibited three 2θ peaks at 0.78°, 1.61° and 1.85°, which can be indexed as (100), (110) and (200) reflections associated with p6mm hexagonal symmetry [60]. Ordered mesoporous carbon had a similar pattern to the SBA-15 template, but with a slight peak shift toward higher 2θ angles (0.98°, 1.80° and 2.03°), suggesting a decreased dimension of the repetitive structure [39]. FOMC showed only one (100) peak at 1.1° with further decreased unit length, which shifted to a higher angle than that of OMC. This suggested that the functionalization had caused slight alternations of the ordered mesoporous structure [61].

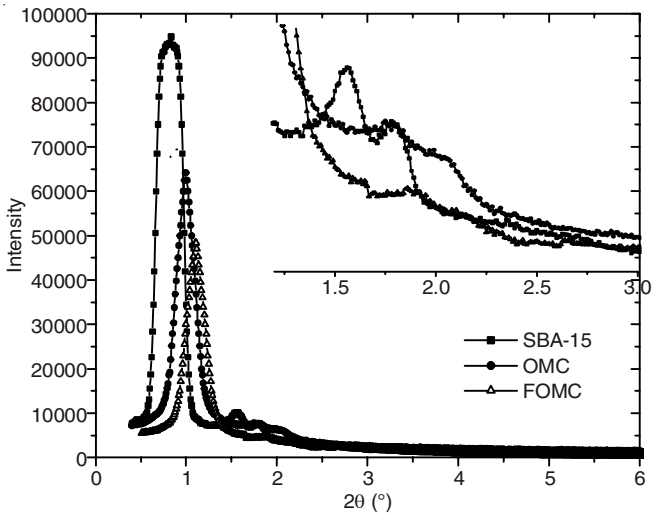

Fig. 3. XRD patterns of SBA-15 and ordered mesoporous carbons

Nitrogen adsorption/desorption isotherms of the mesoporous carbons are presented in Fig. 4. According to the IUPAC classification, the isotherms, in all cases, were of a type IV shape and exhibited a hysteresis loop (Fig. 4A), which is typical of mesoporous materials and suggests the presence of ordered mesoporous structures [62-64]. Based on calculations using the Barrett-Joyner-Halenda (BJH) method, OMC had a surface area of 607 $m^2 g^{-1}$, similar to the SBA-15 template, while the specific surface area of FOMC was 558 $m^2 g^{-1}$ (Table-1). As the relative pressure increased ($p/p^0 > 0.40$), the isotherm of OMC showed a dramatic change in capillary condensation of nitrogen within uniform mesopores, at which the p/p^0 value is related to mesopore diameter. By contrast, FOMC had a constant increase in N_2 adsorption, which is typical of both micro- and mesoporous materials [65] and confirms the reduction in pore size induced by the treatment. The functionalization seemed to result in a slight decline of pore volume from 0.62 to 0.58 $cm^3 g^{-1}$, whereas the average pore diameter was reduced from 4.1 to 3.5 nm (Fig. 4B, Table-1). These measurements were consistent with TEM and XRD characterizations. The reduction of porous structure was likely due to the occupation of functional groups in the internal pores of the OMC [8].

TABLE-1
SURFACE AREA AND PORE PROPERTIES OF ORDERED MESOPOUROUS MATERIALS CALCULATED BY THE BJH METHOD

	BET surface area (m^2/g)	Average pore diameter (nm)	Pore volume (cm^3/g)
SBA-15	609	6.65	1.01
OMC	607	4.10	0.62
FOMC	558	3.80	0.58

The functionalization of OMC with amide groups was confirmed by the FT-IR measurements (Fig. 5). There were several new peaks present for FOMC when compared with OMC. The band occurring at 3740.5 cm^{-1} was ascribed to O-H groups resulting from HNO_3 oxidation, which may enhance the hydrophilic characteristic of OMC and facilitate the surface reactions of chlorination and subsequent amide immobilization. The band at 1722.8 cm^{-1} was assigned to C=O stretching vibrations of non-aromatic carboxyl groups and an aromatic ring stretching coupled to highly conjugated keto groups (9, 16, 17, 18, 21, 40,41, 67). The bands at 1531, 1021 and 556 cm^{-1} resulted from $–NH_2$ and C-N bonds, confirming the presence of amide groups on the OMC surface [66,67]. Measurements

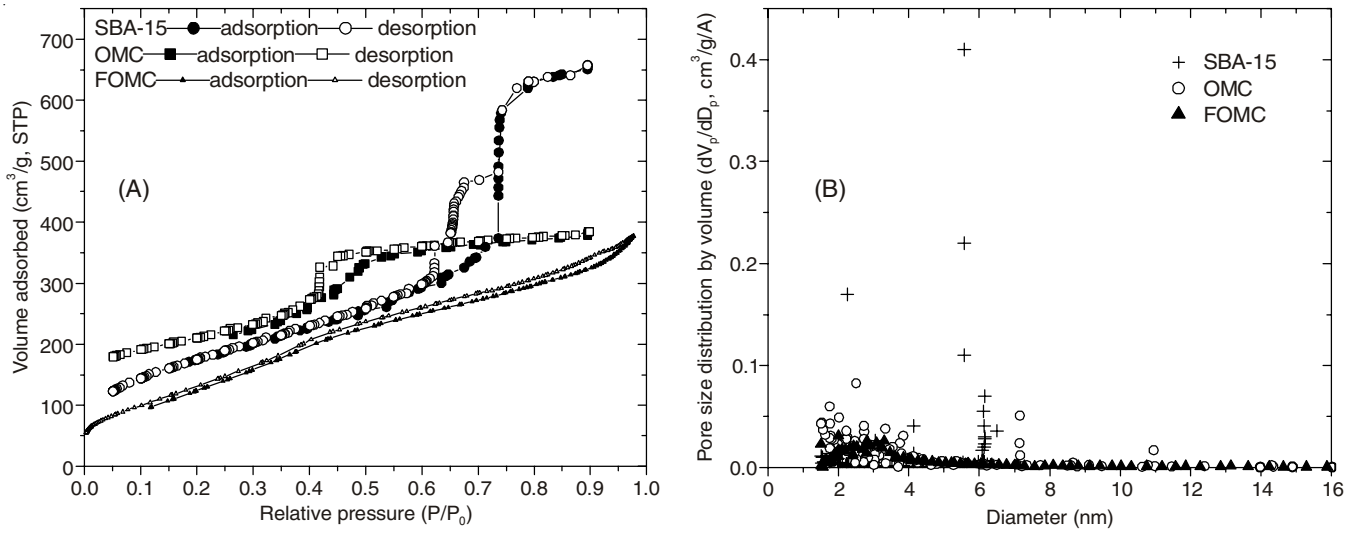

Fig. 4. Nitrogen adsorption/desorption isotherms (A) and the pore size distribution curves (B) of mesopourous materials

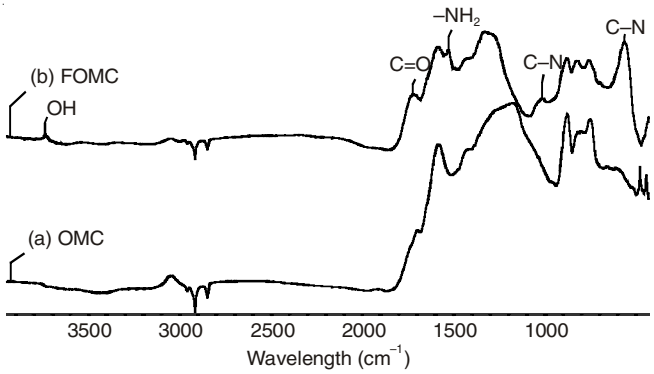

Fig. 5. FT-IR patterns of OMC and FOMC

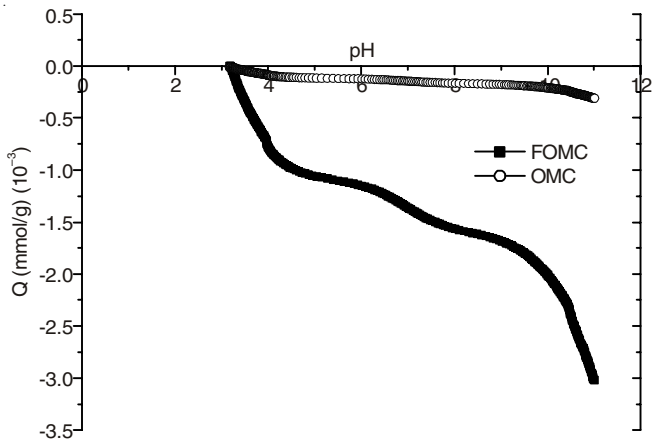

Fig. 6. Net proton-binding isotherms of OMC and FOMC (T = 25 °C, pH = 6.0 and I = 0.01 N $NaNO_3$)

suggest that amide groups had been successfully immobilized onto the OMC surface through the reactions with surface –COOH or –COCl, as illustrated in Fig. 1.

In order to assess the contribution of electrostatic attraction for Hg adsorption and the impacts of the functionalization on surface charges, the proton-binding isotherms of OMC and FOMC were investigated (Fig. 6). Data showed that, in both cases, the surfaces were negatively charged in the systems with pH > 3.1 and became more negative with increasing pH, especially for FOMC. The pHs at the point of zero charge (pH_{pzc}) of OMC and FOMC were measured to be 3.20 and 3.16, respectively. This could be attributed to the presence of negatively charged functional groups on the surface such as ≡COO^- on the surface [68,69]. Higher negative charges on the FOMC surface as induced by the functionalization would favour the electrostatic interactions between metal ions and the surfaces, leading to a rapid adsorption rate and high adsorption capacity [70].

Mercury adsorption

Kinetics: Adsorptive batch experiments with the same OMC and FOMC loading showed similar patterns for Hg removal from the aqueous phase, but FOMC exhibited a stronger affinity for aqueous Hg ions. Mercury removal by FOMC occurred at significantly faster rates and higher capacities than that of OMC. The adsorptive kinetics presented in Fig. 7A indicated that the percentage of Hg^{2+} removal by both carbons increased with time at pH 6.0. The removal occurred rapidly within the first 30 min, then followed by a slower adsorption rate. Within the first 30 min, FOMC removed about 57 and 33 % of total aqueous Hg while OMC removed 38 and 20 %, respectively. There was only a slight increase in the adsorption of mercury afterwards, suggesting that 30 min could be considered an adequate contact time for Hg ion adsorption. Faster adsorption by FOMC suggested a faster mass transfer kinetics and higher affinity of the surface ligands toward Hg ions in comparison with OMC. As expected, there was also a negative correlation between initial Hg concentrations and its percentage removal. Fractional Hg removal was higher with lower initial Hg concentration, though the absolute amount of Hg removed was lower.

Isotherms: The amount of Hg adsorbed at equilibrium (Fig. 7B) indicated that FOMC had a larger adsorptive capacity than OMC. Evidently, the functionalization generated new surface sites for Hg binding [23,71]. Both the Langmuir adsorption isotherm [$q_e = q_0 b c_e/(1 + b c_e)$, C_e is the equilibrium concentration (mg L^{-1}), q_e is the amount adsorbed (mg g^{-1})] and Freundlich isotherm [$q_e = k_f c_e^n$, k_f and n are Freundlich constants, with n indicating how favourable the adsorption process is and k_f (mg g^{-1} (L $mg^{-1})^n$) represents the adsorption capacity of the sorbent] demonstrated that FOMC had

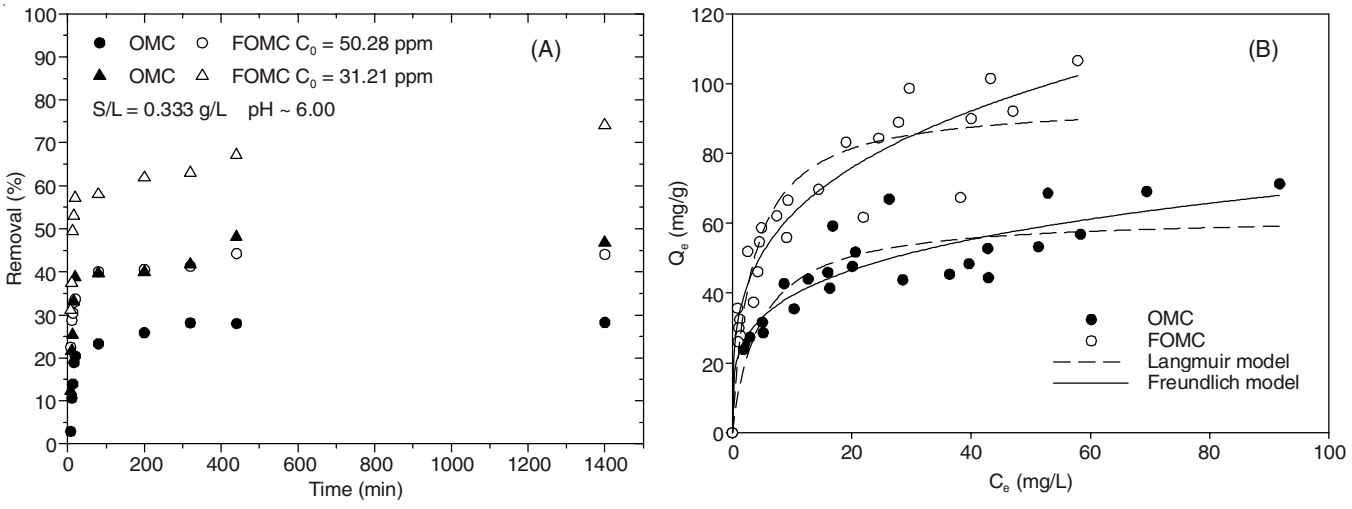

Fig. 7. Mercury adsorptive kinetics (A) and equilibrium isotherm (B) of OMC and FOMC (T = 25 °C, buffer ($KHPO_4$-NaOH) = 0.01 M and pH = 6.0)

TABLE-2
EQUILIBRIUM MODEL CONSTANTS FOR THE Hg^{2+} SORPTION BY OMC AND FOMC

Materials	Langmuir parameters			Freundlich parameters		
	b	Q_0 (mg/g)	r^2	K_f ($mg^{(1-1/n)}L^{1/n}$ g^{-1})	n	r^2
OMC	0.2168	62.11	0.8922	22.18	0.2478	0.9109
FOMC	0.3012	94.80	0.9303	32.65	0.2813	0.9524

approximately 1.5 times higher Hg adsorption capacity than OMC [Fig. 7(B)]. In comparison of two models, Freundlich model had a better fit of data than the Langmuir model, implying that the heterogensous nature of surface sites for Hg adsorption [72-74]. The model constants derived from the two models are listed in Table-2.

pH effect on the adsorption: pH was one of the major factors influencing the adsorption of metal ions. The results on the Hg(II) adsorption experiments onto modified FOMC and unmodified OMC are presented as adsorption edges as a function of pH in Fig. 8 for comparison. We observe that Hg adsorption by FOMC was significantly increased relative to the OMC (96 *vs.* 70 %). In addition, a closer inspection of the FOMC data shows that the improvement starts at lower pH values, a plateau for OMC is established at pH about 5.5~6.5, while in the FOMC the plateau is established earlier, about pH 5 and at a wider pH range 5~7. As mercury adsorbent, this is of specific importance for potential applications of FOMC in Hg remediation in natural waters. The adsorption of Hg onto FOMC and OMC can be modeled (Fig. 8), the adsorption data could be well represented by the diffuse layer model, the set of aqueous and surface reactions used in the modeling were tabulated in Table-3. The WSOS/DF values of FOMC and OMC by FITEQL were 160 and 152 respectively, by assuming Hg(II) binding at the sites, the intrinsic equilibrium constants derived from the fit to the data equals log K= 2.64 (≡$SOHg^+$), 11.19 (≡$XLHg^{2+}$), 7.47 (≡$XLHg(OH)^+$) and –31.51 I(≡$XLHg(OH)_2^0$) for the FOMC, while log K = 14.18 (≡$SOHg^+$), 5.83 (≡XHg(OH)) and –16.90 (≡XHg^+) for the unmodified ordered mesoporous carbon, respectively.

Adsorption mechanisms: The Hg^{2+} adsorption can be accounted for by the aqueous Hg ion speciation shown in Fig. 9. According to the Hg speciation, Hg^{2+} ions are major species at pH < 4 while non-charged $Hg(OH)_2$ are dominant at pH > 4.

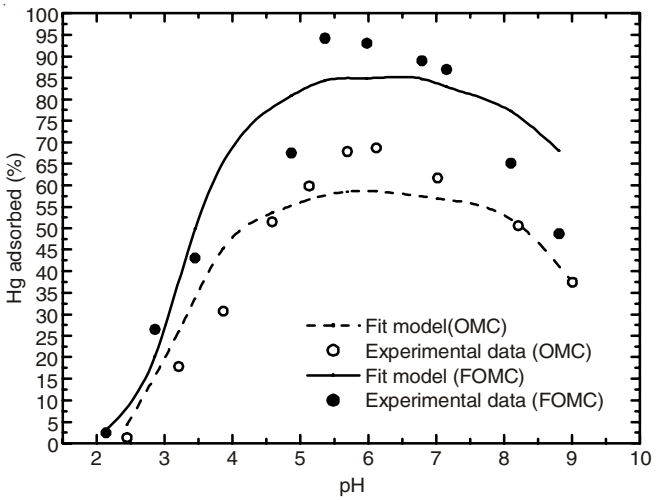

Fig. 8 pH adsorption edges of Hg^{2+} on OMC and FOMC (C_0 = 0.23 mmol L^{-1} and T = 25 °C)

Thus the adsorption at near neutral pH was unlikely a result of the electrostatic interactions [24] and instead, the enhanced Hg adsorption by FOMC could result from the covalent binding of Hg^{2+}, $Hg(OH)^+$ and $Hg(OH)_2$ ions by the surface amide groups as dominant XL-Hg^{2+} species at pH < 4 and XL-$Hg(OH)^+$ species at pH > 4. XL-$Hg(OH)_2$ species could be responsible for the increased Hg adsorption at pH > 6. For OMC, the adsorption was primarily through the permanent charge sites (≡X^-) *via* electrostatic interactions or ion exchange with $Hg(OH)^+$ species, thus non-charged $Hg(OH)_2$ species dominated in equilibrium system.

A conceptual model of Hg adsorptions by FOMC is presented in Fig. 10, where Hg^{2+} reacts with functional groups (≡COO^-, ≡NHR and ≡NH_2) on the surface to form two-, three-, or four-coordinated compounds. Enhanced Hg adsorption by FOMC can be attributed to the amine and amide groups on

TABLE-3
EXPERIMENTAL CONDITIONS, OPTIMIZED REACTIONS AND INTRINSIC EQUILIBRIUM CONSTANTS (log K) USED IN DIFFUSE-LAYER MODEL OF Hg^{2+} ADSORPTION

Total mercury concentration (× 10^{-3} mol/L)	0.23	Hydrolysis reaction	[a]log K
Ligand loading content (× 10^{-3}mol/g)	1.2	$H_2O \leftrightarrow H^+ + OH^-$	13.78
Suspension density in pH edge (g/L)	0.5	$Hg^{2+} + H_2O \leftrightarrow H^+ + Hg(OH)^+$	-2.70
$[SOH]_{OMC}$ concentration (× 10^{-6} mol/L)	1.0	$Hg^{2+} + 2H_2O \leftrightarrow 2H^+ + Hg(OH)_2^0$	-6.19
$[SOH]_{FOMC}$ concentration (× 10^{-3} mol/L)	0.23	$L + H^+ \leftrightarrow LH^+$	9.97
Reactions on OMC-L	[b]log K	$L + 2H^+ \leftrightarrow LH_2^{2+}$	14.16
$SOH + H^+ \leftrightarrow SOH_2^+$	3.50	Reactions on OMC	[b]log K
$SOH \leftrightarrow H^+ + SO^-$	-2.71	$SOH + H^+ \leftrightarrow SOH_2^+$	2.30
$\equiv SO^- + Hg^{2+} \leftrightarrow [\equiv SOHg]^+$	2.64	$SOH \leftrightarrow H^+ + SO^-$	-4.91
$\equiv XL + Hg^{2+} \leftrightarrow [\equiv XLHg]^{2+}$	11.19	$\equiv SO^- + Hg^{2+} \leftrightarrow [\equiv SOHg]^+$	14.18
$\equiv XL + Hg(OH)^+ \leftrightarrow [\equiv XLHg(OH)]^+$	7.47	$\equiv X + Hg(OH)^+ \leftrightarrow [\equiv XHg(OH)]$	5.83
$\equiv XL + Hg(OH)_2^0 \leftrightarrow [\equiv XLHg(OH)_2]^0$	-31.51	$\equiv X + Hg^{2+} \leftrightarrow [\equiv XHg]^+$	-16.90

[a]log K [Ref. 58,59]; [b]log K [This work]

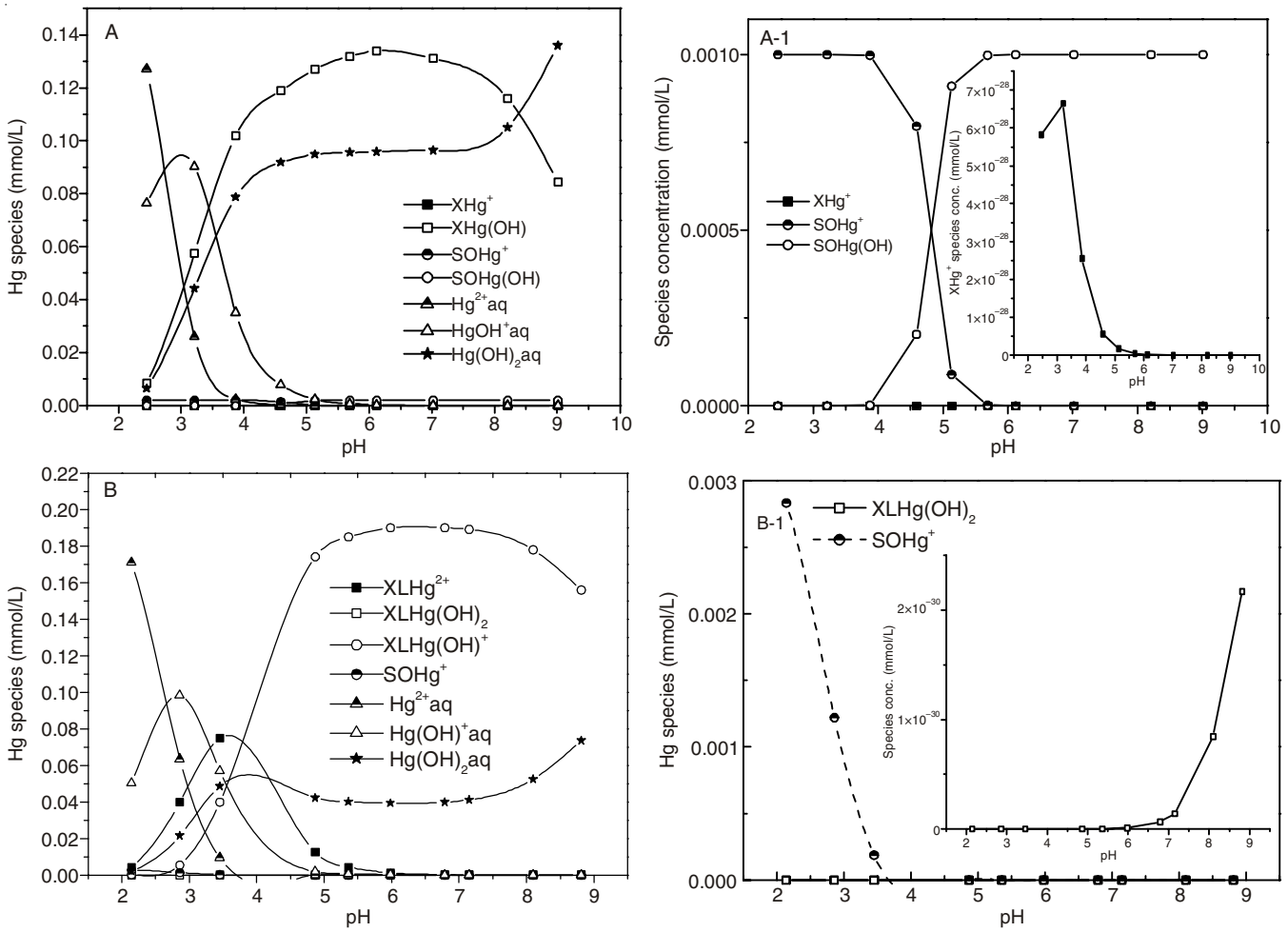

Fig. 9. Theoretical contributions of the Hg^{2+} species in equilibrium system. (A, A-1 for Hg-OMC; B, B-1 for Hg-FOMC)

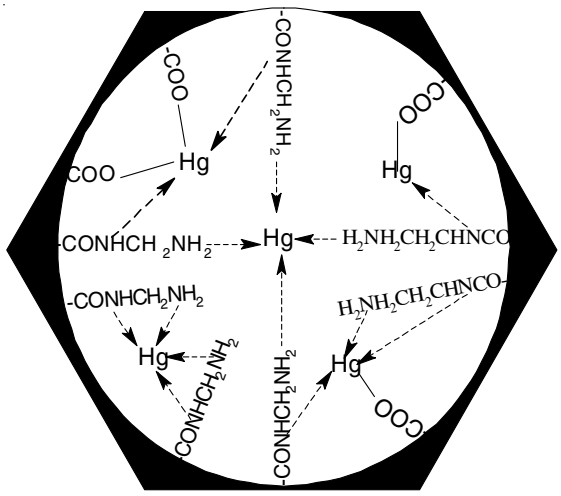

Fig. 10. Schematic illustration of Hg(II) adsorption on FOMC

the surface that form complexes with Hg^{2+} ions through sharing four lone pairs of electrons. Because of its special structures and the outer layer electron clouds, mercury ion has an extraordinary affinity for amide groups and is able to form strong covalent bonds with the groups. The coordination around Hg ions could be through the Hg-N bonds. The strong covalent binding by the ligands plus ordinary Hg^{2+} electrostatic binding could be responsible for increased Hg adsorption [75-77].

Conclusion

In this study, ordered mesoporous carbon was functionalized with amide groups in an effort to enhance Hg removal from aqueous phase. The partial oxidation of the OMC with nitric acid introduced active functional groups on the carbon frameworks, which could then be further modified, *e.g.*, by covalently bonding other molecules. Results of this study demonstrate that it is possible to apply a general method of functionalization and classic organic chemical reactions to modify the OMC surface with desired functionalities, while still largely maintain the original ordered mesoporous structure. Nevertheless, the modifications do change the pore volume and surface charges of carbon to certain degree. The functionalized OMC had significantly enhanced capability to remove aqueous Hg in the context of adsorptive rate, capacity and pH range. Surface complexation modeling provided a detailed analysis of the observed Hg^{2+} binding at all pH values. The diffuse double layer model could describe the Hg^{2+} adsorptions well. The complexation stability constants for forming the surface ≡OMC-Hg and ≡OMCL-Hg complexes could be estimated from the modeling of the experimental data. The functionalizing procedures used in this study are potentially applicable to the development of specific carbon-based adsorbents for removing other aqueous inorganic or organic contaminants.

ACKNOWLEDGEMENTS

Financial support for this research was provided by the USEPA-NCER-STAR (RD831071) and USDA-CSREES (MOX-YANG) to Lincoln University of Missouri, and US-Department of Energy (DE-FC26-02NT41607) to University of Missouri. This work also supported by the Key Natural Science Foundation, transformation mechanism and control principle of nitrogenous pollutant in the urban water supply system (Grant No. 51438006), the National Key Scientific Instrument and Equipment Development Project (Grant No. 2014YQ060773), the Priority Academic Program Development of Jiangsu Higher Education Institutions (RAPD), Colleges and Universities in Jiangsu Province Plans to Graduate Research and Innovation (KYZZ15_0147), Project 948: the water detection system trace volatile organic compounds (30155045912), the Operational Funds for the Central Universities, China (Grant no. 2016B04614).

REFERENCES

1. J. Lee, S. Han and T. Hyeon, *J. Mater. Chem.*, **14**, 478 (2004).
2. S.H. Joo, S.J. Choi, I. Oh, J. Kwak, Z. Liu, O. Terasaki and R. Ryoo, *Nature*, **414**, 470 (2001).
3. Y.S. Fang, X.J. Huang, Q. Zeng and L.S. Wang, *Biosens. Bioelectron.*, **73**, 71 (2015).
4. A. Kondo, A.S. Hall, T.E. Mallouk and K. Maeda, *Chem. Eur. J.*, **21**, 12148 (2015).
5. R. Ryoo, C.H. Ko, M. Kruk, V. Antochshuk and M. Jaroniec, *J. Phys. Chem. B*, **104**, 11465 (2000).
6. J. Brown, R. Richer and L. Mercier, *Micropor. Mesopor. Mater.*, **37**, 41 (2000).
7. R. Anwander, I. Nagl, C. Zapilko and M. Widenmeyer, *Tetrahedron*, **59**, 10567 (2003).
8. Z.M. Gu and B.L. Deng, *Appl. Organomet. Chem.*, **21**, 750 (2007).
9. M.M. Titirici, A. Thomas and M. Antonietti, *J. Mater. Chem.*, **17**, 3412 (2007).
10. R.C. Costello and D.M. Sullivan, *Waste Biomass Valorization*, **5**, 505 (2014).
11. H. Tamai, K. Shiraki, T. Shiono and H. Yasuda, *J. Colloid Interf. Sci.*, **295**, 299 (2006).
12. B. Jarrais, A.R. Silva and C. Freire, *Eur. J. Inorg. Chem.*, **2005**, 4582 (2005).
13. M.L. Cappello, K.A. Hardy, A.R. MacDairmid, M.C. Gallagher and J.T. Banks, *Can. J. Chem.*, **91**, 364 (2013).
14. J. Wang, W.H. Wang, W. Xu, X.H. Wang and S. Zhao, *J. Environ. Sci. (China)*, **23**, 1839 (2011).
15. Y.H. Li, S.G. Wang, Z.K. Luan, J. Ding, C.L. Xu and D.H. Wu, *Carbon*, **41**, 1057 (2003).
16. H. Yoshitake, T. Yokoi and T. Tatsumi, *Chem. Mater.*, **14**, 4603 (2002).
17. H. Yoshitake, T. Yokoi and T. Tatsumi, *Chem. Mater.*, **15**, 1713 (2003).
18. H. Yoshitake, E. Koiso, T. Tatsumi, H. Horie and H. Yoshimura, *Chem. Lett.*, **33**, 872 (2004).
19. B. Lee, Y. Kim, H. Lee and J. Yi, *Micropor. Mesopor. Mater.*, **50**, 77 (2001).
20. A. Bibby and L. Mercier, *Chem. Mater.*, **14**, 1591 (2002).
21. A. Walcarius, M. Etienne, J. Bessiere, Amorphous Silica Gels Grafted with Amine or Thiol Groups, *Chem. Mater.*, **14**, 2757 (2002).
22. Z.H. Xiao, R. Zhang, X.Y. Chen, X.L. Li and T.F. Zhou, *Appl. Surf. Sci.*, **263**, 795 (2012).
23. R.I. Nooney, M. Kalyanaraman, G. Kennedy and E.J. Maginn, *Langmuir*, **17**, 528 (2001).
24. J.Z. Zhu, B.L. Deng, J. Yang and D.C. Gang, *Carbon*, **47**, 2014 (2009).
25. G.P. Jeppu, T.P. Clement, M.O. Barnett and K.K. Lee, *Environ. Eng. Sci.*, **27**, 147 (2010).
26. F.J. Zhang, X.X. Ou, C.Q. Ran and Y.N. Wu, *Adv. Mater. Res.*, **255-260**, 2810 (2011).
27. S. Kumar, S.V. Godbole and B.S. Tomar, *Radiochim. Acta*, **101**, 73 (2013).
28. J.H. Pan, R.X. Liu and H.X. Tang, *J. Environ. Sci. (China)*, **19**, 403 (2007).
29. A. Kriaa, N. Hamdi and E. Srasra, *J. Struct. Chem.*, **50**, 273 (2009).
30. V. Gupta, S.J. Liu, H. Ando, R. Ishii, S. Tateno, Y. Kaneko, M. Yugami, S. Sakamoto, Y. Yamaguchi, O. Nureki and H. Handa, *Mol. Pharmacol.*, **84**, 824 (2013).
31. M. Berka and I. Banyai, *J. Colloid Interf. Sci.*, **233**, 131 (2001).
32. H. Roohi and M. Jahantab, *Comput. Theoret. Chem.*, **1066**, 76 (2015).
33. C. Foti, O. Giuffre, G. Lando and S. Sammartano, *J. Chem. Eng. Data*, **54**, 893 (2009).
34. J.P. Chen and M.S. Lin, *Carbon*, **39**, 1491 (2001).
35. C.L. Chen, J. Hu, D. Xu, X.L. Tan, Y.D. Meng and X.K. Wang, *J. Colloid Interf. Sci.*, **323**, 33 (2008).
36. C.S. Yuan, G.Z. Wang, S.H. Xue, I.R. Ie, Y.H. Jen, H.H. Tsai and W.J. Chen, *J. Air Waste Manage.*, **62**, 799 (2012).
37. A. Kotland, S. Chollet, J.M. Autret, C. Diard, L. Marchal and J.H. Renault, *J. Chromatogr. A*, **1391**, 80 (2015).
38. M. D'Arcy, F. Bullough, C. Moffat, E. Borgomeo, M. Teh, R. Vilar and D.J. Weiss, *J. Chem. Educ.*, **91**, 505 (2014).
39. Z.M. Gu, B.L. Deng and J. Yang, *Micropor. Mesopor. Mater.*, **102**, 265 (2007).
40. W. Yantasee, Y.H. Lin, G.E. Fryxell, K.L. Alford, B.J. Busche and C.D. Johnson, *Ind. Eng. Chem. Res.*, **43**, 2759 (2004).
41. T.J. Lund, C.M. Koretsky, C.J. Landry, M.S. Schaller and S. Das, *Geochem. Trans.*, **9**, 9 (2008).
42. C. Bretti, C. De Stefano, G. Lando and S. Sammartano, *Fluid Phase Equilib.*, **355**, 104 (2013).
43. Y. Zhang, Z.F. Ye, L.Y. Wang, L.Q. Yang and Y.F. Li, *Desalination Water Treat.*, **52**, 6481 (2014).
44. G. De Tommaso and M. Iuliano, *J. Chem. Eng. Data*, **57**, 52 (2012).
45. B. Zou, Y. Hu, F.J. Cui, L. Jiang, D.H. Yu and H. Huang, *J. Colloid Interf. Sci.*, **417**, 210 (2014).
46. X.L. Zhao, T. Jiang and B. Du, *Chemosphere*, **99**, 41 (2014).
47. M.Q. Wei, Y.G. Duan, Q.T. Fang, R. Wang, B.M. Yu and C.S. Yu, *J. Central South Univ.*, **20**, 1928 (2013).
48. G. Balomenou, P. Stathi, A. Enotiadis, D. Gournis and Y. Deligiannakis, *J. Colloid Interf. Sci.*, **325**, 74 (2008).
49. E. Giannakopoulos, P. Stathi, K. Dimos, D. Gournis, Y. Sanakis and Y. Deligiannakis, *Langmuir*, **22**, 6863 (2006).
50. K. Subramaniam, V. Vithayaveroj, S. Yiacoumi and C. Tsouris, *J. Colloid Interf. Sci.*, **268**, 12 (2003).
51. M.M. Liu, L.A. Hou, B.D. Xi, Y. Zhao and X.F. Xia, *Appl. Surf. Sci.*, **273**, 706 (2013).
52. R. Bouchet, D. Devaux, V. Wernert and R. Denoyel, *J. Phys. Chem. C*, **116**, 5090 (2012).
53. J. Chan, A. Lu and A.J. Bennet, *J. Am. Chem. Soc.*, **133**, 2989 (2011).
54. J. Ikhsan, M.J. Angove, B.B. Johnson and J.D. Wells, *J. Colloid Interf. Sci.*, **284**, 400 (2005).
55. P. Zhou, H. Yan and B.H. Gu, *Chemosphere*, **58**, 1327 (2005).
56. Y. Gopalapillai, C.L. Chakrabarti and D. Lean, *Environ. Chem.*, **5**, 307 (2008).
57. D.K. DeForest and E.J. Van Genderen, *Environ. Toxicol. Chem.*, **31**, 1264 (2012).
58. D. Sarkar, M.E. Essington and K.C. Misra, *Soil Sci. Soc. Am. J.*, **64**, 1968 (2000).
59. A.P. Cochrane, C.G. Merrett, H.H. Hilton, The Influence of Time Dependent Flight and Maneuver Velocities and Elastic or Viscoelastic Flexibilities on Aerodynamic and Stability Derivatives, 10th International Conference On Mathematical Problems in Engineering, Aerospace and Sciences (ICNPAA 2014), vol. 1637, pp. 403-412 (2014).
60. D.Y. Zhao, Q.S. Huo, J.L. Feng, B.F. Chmelka and G.D. Stucky, *J. Am. Chem. Soc.*, **136**, 10546 (2014).
61. X. Du and G.-H. Yang, *Int. J. Control*, **82**, 1485 (2009).
62. D.Y. Zhao, J.Y. Sun, Q.Z. Li and G.D. Stucky, *Chem. Mater.*, **12**, 275 (2000).
63. S. Jun, S.H. Joo, R. Ryoo, M. Kruk, M. Jaroniec, Z. Liu, T. Ohsuna and O. Terasaki, *J. Am. Chem. Soc.*, **122**, 10712 (2000).
64. M. Kruk, K.M. Kohlhaas, B. Dufour, M. Jaroniec, K. Matyjaszewski, E.B. Celer, R.S. Ruoff and T. Kowalewski, *Micropor. Mesopor. Mater.*, **102**, 178 (2007).
65. Y.Q. Li, B.P. Bastakoti, M. Imura, N. Suzuki, X.F. Jiang, S. Ohki, K. Deguchi, M. Suzuki, S. Arai and Y. Yamauchi, *Chem. Asian J.*, **10**, 183 (2015).
66. R.A. Khatri, S. Chuang, Y. Soong and M. Gray, *Ind. Eng. Chem. Res.*, **44**, 3702 (2005).
67. A. Chang, S. Chuang, M. Gray and Y. Soong, *Energy Fuels*, **17**, 468 (2003).

68. A.D. Pomogailo, *Polym. Sci. Ser. C*, **48**, 85 (2006).
69. A. Stein, B.J. Melde and R.C. Schroden, *Adv. Mater.*, **12**, 1403 (2000).
70. C.Y. Lu and H.S. Chiu, *Chem. Eng. Sci.*, **61**, 1138 (2006).
71. H. Bessbousse, J.F. Verchere and L. Lebrun, *Chem. Eng. J.*, **187**, 16 (2012).
72. T. Padmesh, K. Vijayaraghavan, G. Sekaran and M. Velan, *Chem. Eng. J.*, **122**, 55 (2006).
73. T. Akar, S. Celik, A. Gorgulu Ari and S. Tunali Akar, *J. Chem. Technol. Biotechnol.*, **88**, 680 (2013).
74. M.A. Hughes and E. Rosenberg, *Sep. Sci. Technol.*, **42**, 261 (2007).
75. D. Lafont, O.E. Soulages, S.G. Acebal and A.G. Bonorino, *Environ. Earth Sci.*, **70**, 1379 (2013).
76. L. Zong and C.C. Chen, *Fluid Phase Equilib.*, **306**, 190 (2011).
77. M.S. Bharara, S. Parkin and D.A. Atwood, *Inorg. Chem.*, **45**, 7261 (2006).